

UAV imagery based tree species classification in the Marburg OpenForest

Darius G3rgen () Tobias Koch () Marvin M3sngen () Eike Schott ()

April 17, 2020

Abstract

The monitoring of forests environments is of crucial importance since they serve as natural habitats and constitute a main source of biological diversity on the planet. Yet, it is very costly and labor intensive to monitor forests by traditional means and classical remote sensing technologies restrict the analysis to the regional level. To overcome these challenges there have been several attempts to use UAV-borne imagery in forest monitoring. By the use of drones images can be obtained at low cost and can be associated with both, high spatial and temporal resolution. This enables scientists and practitioners to comprehensively monitor forest environments. In this paper we present our results of an experiment exploring the influence of spatial resolution of RGB imagery, artificially derived vegetation indices as well as seasonal parameters on the accuracy of tree species classification within the Marburg OpenForest. We used a resolution of 10, 15, and 25 cm in a forward-feature-selection based on the Random Forest classification algorithm. Additionally we tested the obtained accuracy when only mono-temporal or multi-temporal variables are included as well as both types of variables. Our results show that accuracy is prone to errors in pixel georeferencing and tree location. Object-based classification methods might lead to higher classification accuracies, but the construction of balanced training dataset is of preliminary importance and needs further improvement for our study area, where we yield to an overall accuracy of 64.8% for a pixel-wise classification based on a combination of mono-temporal and seasonal predictors.

Contents

| | | |
|----------|---|-----------|
| 1 | Introduction | 2 |
| 2 | Data and Methods | 3 |
| 2.1 | Study Area | 3 |
| 2.2 | Pre-Processing of the UAV orthoimages | 4 |
| 2.3 | Tree species data | 6 |
| 2.4 | RGB indices | 6 |
| 2.5 | Classification and Validation | 8 |
| 3 | Results | 9 |
| 4 | Discussion & Conclusion | 12 |
| | References | 13 |

1 Introduction

Forests environments provide valuable services to the human well being as well as supporting services to the function of ecosystems. Additionally, they count to the main biodiversity hotspots on earth (Brockerhoff et al., 2017). However, the most recent Global Forest Resource Assessment of the FAO states, that the global forest area shrunk between 1990 and 2015 from 31.6% of the global land cover to 30.6%, or in other numbers from 4,128 Mio. ha to 3,999 Mio. ha - a decrease of 3.1% (Food and Agriculture Organisation of the United Nations, 2015). Simultaneously, the percentage of planted trees increased by over 105 Mio. ha, reducing the share of natural forest areas. Over the last decades, we can find growing scholar interests on ecosystem services and functions which are sustained by forests, mainly the habitat provision for endangered or native species, the provision of material goods such as wood biomass, soil formation and composition, as well as climatic regulation functions, such as carbon sequestration (Brockerhoff et al., 2017). One of the main critical variables in assessing the quality of forest environments, their biodiversity, and their structural attributes is the tree species, either on the individual tree level or the dominating species for coarser areas of interest.

Identifying tree species, however, on an operative scale for larger areas, remains a challenge. Recently, different remote sensing approaches proved that tree species identification from above the earth’s surface is feasible, but there still remain significant trade-offs between the costs, computational demand and spatial-temporal resolution of remotely sensed imagery. Some studies have used satellite imagery which most frequently also include information in the infrared spectrum (Elatawneh et al., 2013; Grabska et al., 2019; Persson et al., 2018; Ulsig et al., 2017; Zhang et al., 2003) but generally shows a relatively low spatial resolution limiting the analysis to a level of stand rather than individuals. Additionally, depended on the platform’s orbit and current weather conditions, the temporal resolution may vary significantly and is not completely planable.

One technology to partly overcome these restrictions is the use of Radio Detection And Ranging (RADAR) sensors which show a lower dependency of data quality to the presence of clouds and fog. Recently, multi-temporal data from Sentinel-1 has been used in conjunction with spectral data to not only improve the species classification accuracy but also to retrieve additional parameters important to forest monitoring such as forest type, stand density, annual phenology, and biomass production among others (Dostálová et al., 2018; Frison et al., 2018; Mngadi et al., 2019; Niculescu et al., 2018). However promising these advances, the analysis are most commonly restricted to regional analysis of forest structures. On a more localized level, high resolution satellite data is either not available or associated with very high costs. With the rapid development of unmanned aerial vehicles (UAV) during the last years and a significant decrease in price for this technology, new approaches to monitor forest structures on a very local level have recently emerged (Yao et al., 2019).

UAVs serve as an aerial platform of different kind of sensors which can range from LidAR (Fricker et al., 2019), hyper- and multi spectral sensors (Berra et al., 2019; Marques et al., 2019) as well as simple RGB cameras (Natesan et al., 2019). A broad methodology to obtain species information for single tree individuals has been developed integrating the calculation of various vegetation indices from mono- and multi-temporal imagery and the use of machine learning models to derive a relationship between the measured variables and the tree species. Berra et al. (2016) used the Green Chromatic Coordinate to monitor the Start-of-Season for four different tree species in deciduous woodland suggesting that UAV imagery can contribute to investigate the phenological status of individual trees. Klosterman and Richardson (2017) were able to estimate phenological status on the leaf-level based on the calculation of the green and red chromatic coordinate (GCC and RCC) during spring and autumn to model bud burst and leaf expansion as well as leaf senescence. Natesan et al. (2019) used Residual Neural Networks to classify three different tree species based on RGB imagery obtained over the course of three years and achieved a classification accuracy of about 80%, and an accuracy of 51% when only the data of single years was used. Fricker et al. (2019) used hyperspectral images obtained by a UAV and a Convolutional Neural Network to classify tree species. They also underwent an experiment which only included RGB data. The hyperspectral data achieved an F-score of 0.87, while the RGB data achieved a score of 0.64 in a dominantly coniferous forest.

Additionally, the development of structure-from-motion algorithms to get 3D information from 2D RGB imagery taken from slightly different angles have enriched the analysis of forest structures from low-cost sensors. Nevalainen et al. (2017) used RGB images and an automated matching technique to obtain point

clouds at a 5cm resolution. Coupled with hyperspectral imagery this allowed the tree species classification to an accuracy at 95%. Yan et al. (2018) compared their approach of retrieving tree crowns from RGB images with crowns delineated from LiDAR data and report an accuracy at about 90%. Krause et al. (2019) were able to retrieve individual tree height based on a photogrammetric point-cloud with an RMSE at about 2-3 %. Brieger et al. (2019) used RGB derived point clouds at different study sites in Siberia and achieved an accuracy of 67.1% in delineating individual tree crowns and an RMSE of 18.46% for tree height. Sothe et al. (2019) used hyperspectral images for tree delineation and classification in subtropical rain forests and achieved a Kappa score of 0.7 (overall accuracy of 72.4%) by combining spectral raw data, indices as well as structural parameters in the classification process using a support-vector machine. Richardson et al. (2009) proved, that simple RGB images can contribute to seasonally differentiate tree green-up and senescence in different forest environments.

However, little efforts have been done to structurally investigate the impact of decreasing spatial resolution on the classification accuracy as well as the impact of the integration of seasonal parameters derived from multiple mono-temporal observations. Here, we strictly limit our analysis to the investigation of these two thematic blocs and deliberately exclude other factors such as structural variables obtained from point clouds. We solely focus on the analysis of the dynamic in predictive potential of RGB derived mono- and multi-temporal variables to model tree species with changing spatial resolution.

To this end we use the RGB imagery obtained by multiple overflights during the year 2019 from a study site located within the Marburg University forest which is part of the research project Natur 4.0. This forest is used as a joint research area for a project between several German universities and research institutes and sets out to investigate the potential of sensor technology for biodiversity and natural resource management in natural forest environments. We artificially decreased the spatial resolution of aerial imagery obtained in this area resulting in three different target resolutions of 10, 15, and 25 cm. For every single overflight we calculated a series of RGB indices on a pixels basis. Additionally, we calculated descriptive statistics (mean, maximum, minimum, amplitude, etc.) for each index over the course of the year to include information about the seasonality of the phenological development.

The resulting input data is used to establish a total of nine distinct random forest models, one for each resolution including either only mono-temporal or seasonal predictor variables or both types of variables. On the basis of a forward-feature selection the variables which carry the most relevant information content for the tree species classification are then selected and used in the species prediction. The evaluation of the classification accuracies is compared on a pixel and object basis to draw conclusions on the importance of spatial resolution as well as the importance of mono- vs. multi-temporal input data.

2 Data and Methods

2.1 Study Area

The study area is located at 50.8°N 8.7°E in the German low mountain range in Hessen. It is part of the University Forest Caldern where the recently initiated joint research project Natur 4.0 aims at investigating the use of networked sensor technology for biodiversity and ecosystem management and protection. It is in this context, that the aerial images which we used here were obtained in an observation campaign during 2019 (see Tab. 1). The area is approximately 37,500 m² and continuously covered by trees. In this specific location, only two distinct species are present with stem diameters at breast height (DBH) greater than 40 cm, namely *fagus sylvatica* and *quercus robur*.

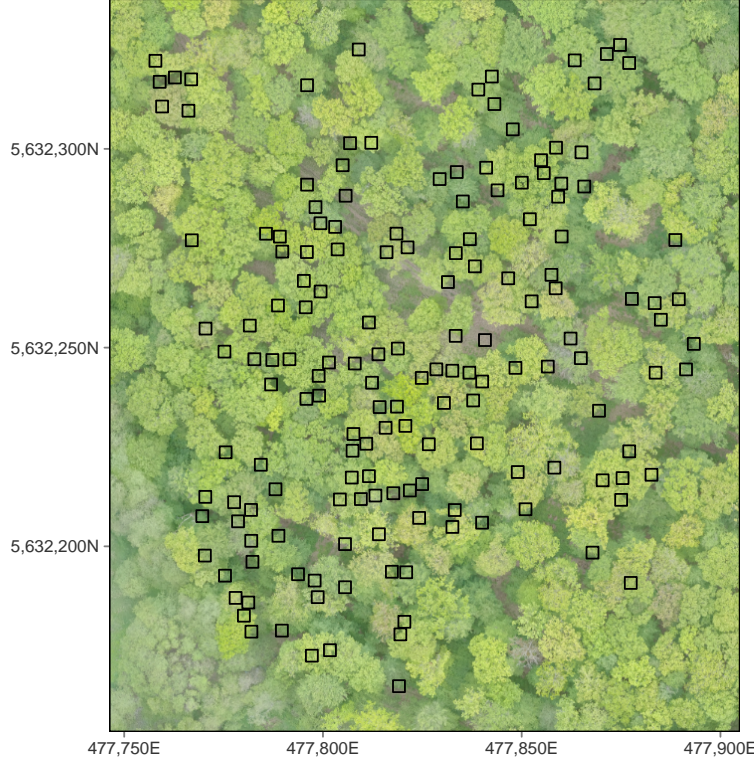


Figure 1: RGB image of the study area from May 16th 2019 with central positions of tree stems superimposed (Coordinates are presented in UTM32N).

2.2 Pre-Processing of the UAV orthoimages

In this project, AgisoftPhotoScan was used to process the UAV imagery. Agisoft Photoscan Professional is an affordable 3D reconstruction software from the Russian company Agisoft LLC Agisoft (2019) for the generation of dense point clouds and photogrammetric products such as orthorectified mosaics and digital surface models (DSM) derived from point clouds. Photoscan has the advantage to provide a simple workflow, from performing bundle block adjustment to calibrate the camera and orientate images after automatic tie point measurements, geo-referencing by measuring ground control points, concluding with the computation of a dense point cloud and requested final products (Mayer and Kersten, 2018). An airborne system was used to acquire the imagery using a commercial GoPro in several flight campaigns with a flight altitude of 40 meters. The internal GPS of the GoPro was used for geotagging the images. A post referencing enabled a better processing of the images in SFM software and more accurate orthophotos without manual referencing in Photoscan. Photo Alignment is a process in PS for image matching and bundle block adjustment in an arbitrary system. It generates a sparse point cloud as well as the interior and exterior orientation parameters of all images in that system, including systematic error compensation such as non-linear lens distortions. Prior to the adjustment, the tie points are automatically measured by detecting and matching features in overlapping images resulting in a sparse point cloud (Mayer and Kersten, 2018). The settings in this project were chosen as follows:

- General: Accuracy: Medium; Generic preselection: yes; Reference preselection: yes
- Advanced: Key Point limit: 40000; Tie point limit: 4000; apply mask: no; Adaptive camera model fitting: yes

Sparse cloud filtering was performed under the following settings:

- gradual selection: reprojection error: 0.26; reconstruction uncertainty: 189.461; projection accuracy: 12.4621; reconstruction uncertainty: 6.72951; reprojection error: 0.122199

Table 1: **Dates** of the UAV overpasses.

| Dates |
|------------|
| 2019-04-29 |
| 2019-05-03 |
| 2019-05-10 |
| 2019-05-16 |
| 2019-06-05 |
| 2019-06-20 |

Based on the information of the point cloud PhotoScan can construct a polygon model (e.g. mesh) (Agisoft, 2019). In this project the mesh was build by the following settings:

- General: surface type: Height field (2.5D); source data: sparse cloud; face count: medium
- Advanced: interpolation: enabled; point classes: all; calculate vertex colors: no

The different pixel values from different photos are combined by the mosaic type in the final texture. Mosaic type implies a two-step approach. Low frequency components are blended for overlapping images to avoid seam line problems. The high-frequency component, on the other hand, which is responsible for the image details, is only captured from a single image.

In total we worked on 6 images which were obtained between the end of April to the end of June (see Table 1). In the mid latitudes of central Europe these are the months of vegetational peak of mixed forests. However, it must be noted, that the images provided by the Nature 4.0 project showed a rather large margin of error when it comes to the accuracy of georeferencing Therefore, a number of locations in the images are not optimally overlaid, which leads to image distortions. The following figure shows the image distortion for a sample location. This location is not included in our study area, where we suggest the difference of localization to be much smaller than in the image below. However, we could not exclude the influence of these distortions completely.



Figure 2: Display of the image distortion in the data basis (The car as well as the rectangle form on the right of the image are visible multiple times at slightly different locations due to the construction of the mesh).

2.3 Tree species data

With the use of a differential GPS the position of tree stems within the study area was logged during a field campaign. Associated with the positional data, the tree species as well as the DBH was collected. As stated before, here we only focused on the determination of the impact of changing resolutions and multi-temporal predictor variables on the classification accuracy. Therefore, we simplified the delineation of tree crowns corresponding to the needs of the investigation. First, we excluded all trees with a DBH below 40 cm, because we assumed that the crowns of greater trees would cover the smaller ones and thus they could not be observed on aerial images from above the crown surface. Secondly, we buffered the central positions of the residual trees by a square of 2 x 2 m, assuming that with this size we would essentially cover substantial proportions of the associated tree crown (Fig. 1). However, some of these buffered polygons intersected. In these cases, we decided to exclude both intersecting polygons since any decision to keep one over the other would be arbitrary. In the end, we obtained 161 tree individuals of which 92 (57%) were *fagus sylvatica* and 69 (43%) were *quercus robur*.

2.4 RGB indices

We calculated a number of seven color vegetation indices (VI) which can be found in Table 2. These color indices were suspected to care information content on the phenological development of tree species during a year. Indices are frequently used in remote sensing studies due to their relational nature which compensates for influences of illumination and viewing geometry on the measured reflectance values of the RGB channels. The chosen indices delivered satisfying results in prior studies, which corresponding sources are reported in Table 2. They were calculated for each UAV overpass resulting in $(7VIs+R+G+B) \times 6$ observations = 60 mono-temporal predictor variables. Additionally, we calculated the maximum (MAX), minimum (MIN), sum (SUM), standard deviation (SD), amplitude (AMP) as well as the 25%- (Q25) and 75%-percentile (Q75) values for each VI and the RGB channels and the raw channels across the time series resulting in additional 70 seasonal predictors.

Table 2: Names and formulas of RGB indices.

| name | abbreviation | formula | reference |
|----------------------------|--------------|---|--|
| Triangular greenness index | TGI | $-0.5 * (190*(R-G) - 120*(R-B))$ | Broge and Leblanc (2001) |
| Green Leaf Index | GLI | $(2*G-R-B) / (2*G+R+B)$ | Gobron et al. (2000) |
| Color Index of Vegetation | CIVE | $(0.441*R-0.881*G + 0.385*B + 18.787)$ | Wan et al. (2018) |
| Iron Oxide Index | IO | R/B | Rowan and Mars (2003) |
| Visible Vegetation Index | VVI | $(1- R-30 / R+30) * (1- G-50 / G+50) * (1- B-1 / B+1)$ | Planetary Habitability Laboratory (2015) |
| Green Chromatic Coordinate | GCC | $G / (R+G+B)$ | Sonnentag et al. (2012) |
| Red Chromatic Coordinate | RCC | $R / (R+G+B)$ | Richardson et al. (2009) |

Note:

R: 580-670 nm, G: 480-610 nm, B: 400-520 nm, for digital cameras according to Hunt et al. (2012).

Fig. 3 shows the trajectory of the calculated VIs according to the tree species indicating the mean value (points) as well as \pm one standard deviation from the mean (vertical bars) based on all pixels within the respective tree polygons per class. The trajectories are very similar for both classes, however, for almost all VIs there are substantial differences between the classes during the first few observations from April to May. We also see, that between the 16th of May and the 5th of June, we have a relatively large period with no observations.

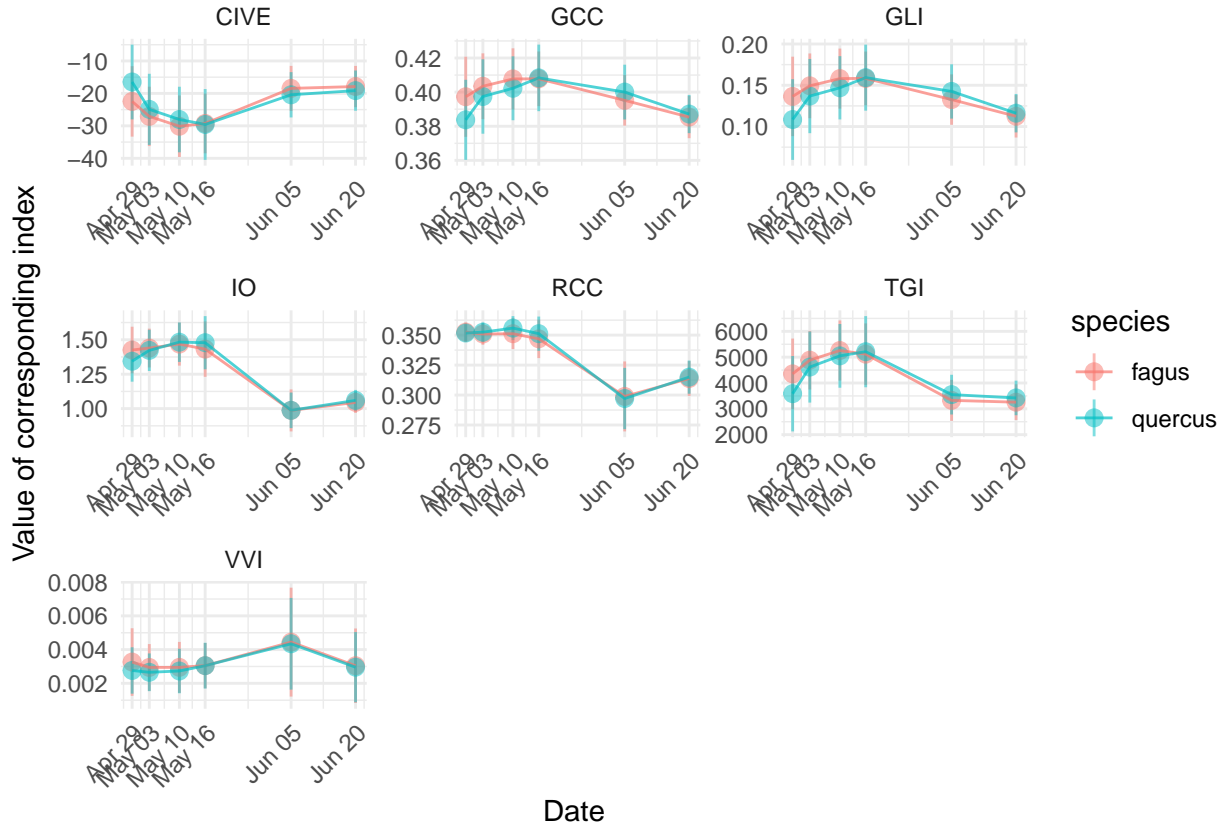


Figure 3: Temporal dynamic of calculated VIs over the course of the year by tree species at 25 cm resolution (points represent the average value, the bars represent +/- one standard deviation).

Concerning the frequency of the seasonal predictor variables both tree species are characterized by a very similar distribution (Fig. 4), however, we see that we have a substantially higher number of pixels classified as *fagus sylvatica* in total.

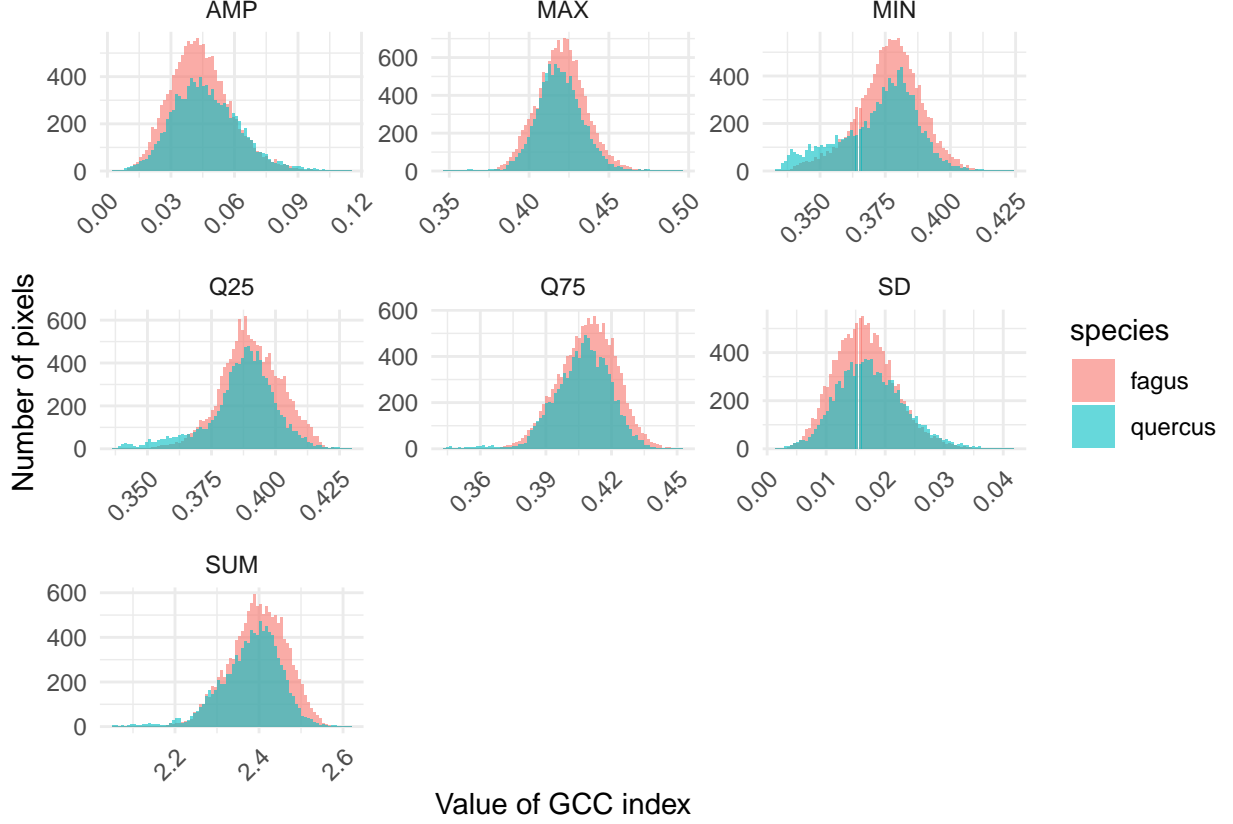


Figure 4: Exampalry histogramm plot of seasonal parameters for RCC by tree species at 25 cm resolution.

2.5 Classification and Validation

For the classification of tree species we used a Random Forest model based on a forward-feature selection of predictor variables stratified by a leave-location-out five-fold cross-validation technique (LLOCV). Random Forest is a non-parametric model, both suitable for regression and classification problems. It was developed by Breiman (2001) and it works by the establishment of a number of decision trees, the forest, each constructed on a random split of predictor variables. The final class decision is made by a majority vote of all trees in the forest. We used the implementation in the `caret` package (Kuhn, 2019) as well as the `CAST` package to implement the LLOCV (Meyer, 2018).

To validate the models, the overall accuracy (OA) is determined. OA describes the number of correctly classified observations divided by the total number of observations and is used in a number of studies to determine the validity of classification models (Natesan et al., 2019; Onishi and Ise, 2018; Sothe et al., 2019). As a another statistical measure of quality, the accuracy of species classification on an object basis is investigated. An object is considered correctly classified if a majority of the pixels belonging to the object corresponds to the class of this object. Here we consider the 2m x 2m squares around each GPS point as an representation of the corresponding tree object. Since we did not used a tree crown delineation, this is an over-simplistic object definition, thus we refer to it as a pseudo-object classification form here on.

To generate further insights into the importance of single variables and indices, we evaluated the variable importance. The variable importance describes the explanatory portion a variable has in a given model in percent. The variable with the highest explanatory share is set to 100% and the explanation share of the remaining variables is shown in relation to this variable with the highest explanation power, thus indicating percentages below 100%.

3 Results

Figure 5 shows that all models regardless of the predictor combination and resolution, show an averaged OA across all folds below 65%. The averaged OA slightly increases for all predictor combinations with a decrease in the spatial resolution, yielding to the highest accuracies at a resolution of 25 cm. The comparison reveals that the models calculated exclusively with mono-temporal indices show a substantially higher OA than the models calculated exclusively with seasonal indices (~3%). The inclusion of both, mono-temporal and seasonal parameters, increases the OA at a rate of about ~1%. For the 15 cm resolution, we observe that for all predictor combinations the margin between the folds of the cross-validation is the largest, ranging between 55% to 74.8%. The margin of accuracies across the folds is the smallest at a resolution of 25 cm for all predictor combinations.

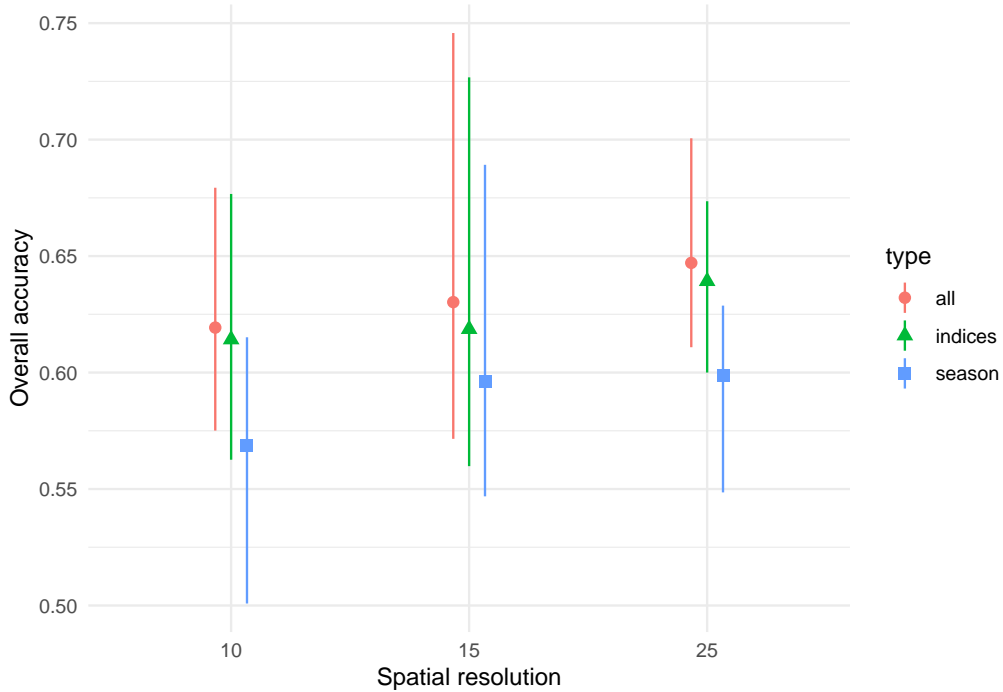


Figure 5: Overall accuracy of the 5-fold cross-validation based on varying pixel sizes and predictor variables (green - mono-temporal indices, blue - seasonal indices, red - mono-temporal and seasonal indices)

Figure 6 shows the OA of the pseudo-objects classified as the correct species based on the majority of pixels within its boundaries. It is clearly shown that, regardless of the variables used, the accuracy of pseudo-object classification increases from a resolution of 10 cm to a resolution of 15 cm. At a resolution of 20 cm, on contrast, we either observe a negative effect or no effect at all on the OA of the models. Especially for mono-temporal predictors, we observe an decrease of OA from 94.8% to 89.1% (-5.7%). It is also evident from the figure that the models where a combination of mono-temporal and seasonal indices were used had the lowest accuracy in an object-based classification but achieved the highest OA on a pixels basis (Figure 5).

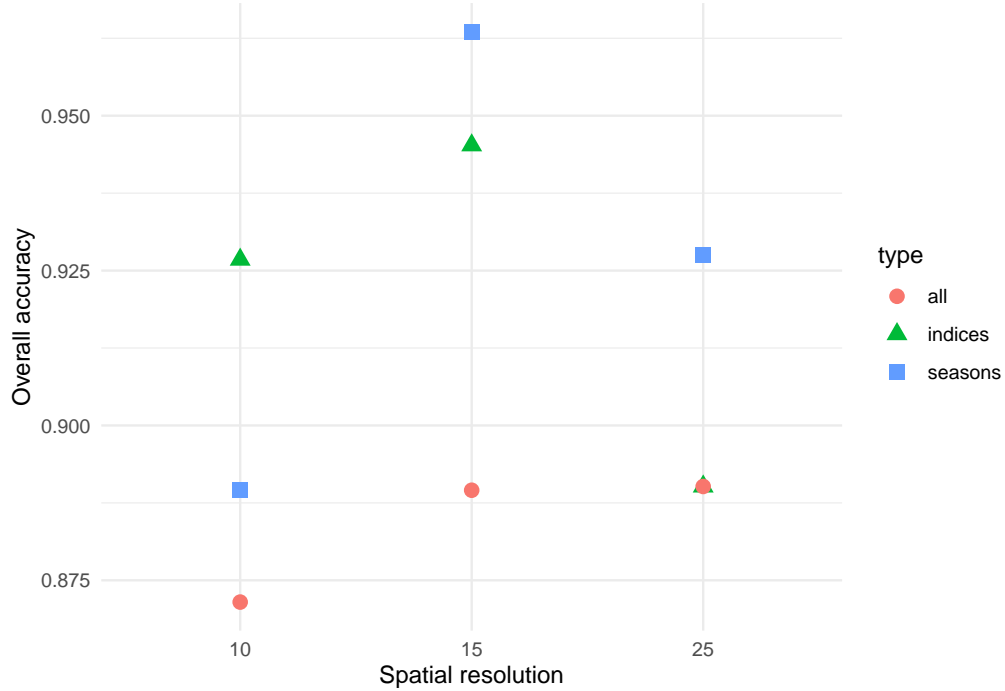


Figure 6: Overall Accuracy of species classification on an pseudo-object basis.

Figures 7 and 8 show the predictors and their relative explanatory power for the models with mono-temporal indices, seasonal indices and both variable types in combination. The explanation percentages of the individual predictors were calculated from the respective models.

For models with mono-temporal predictors, the GCC, GLI and VVI indices are of particular high importance (Fig. 7). It is noticeable that the aerial photographs of June 5th play an important role in the model calculation. When seasonal predictors are used for model calculation, Figure 8 shows that the RCC index is of great importance. Also, seasonal parameters of the TGI appear three times.

Looking at the explanatory share for models calculated using a combination of mono-temporal and seasonal indices (Fig. 8), it is noticeable that significantly more mono-temporal predictors are important than seasonal predictors. Furthermore, it can be seen that the importance of mono-temporal predictors for model explanation changes in comparison to Figure 7. However, it is observed that the GCC index of April 29th is of higher importance compared to the mono-temporal predictors models only. In addition, completely different predictors, irrespective of whether they are mono-temporal or seasonal, have an influence on the model explanation than in the models with exclusively mono-temporal or seasonal predictors. The importance of predictors for June 5th, however, remains also in the combination models. The situation is similar for the GCC, RCC and VVI indices, which are more frequently present as high importance explanatory variables than other indices.

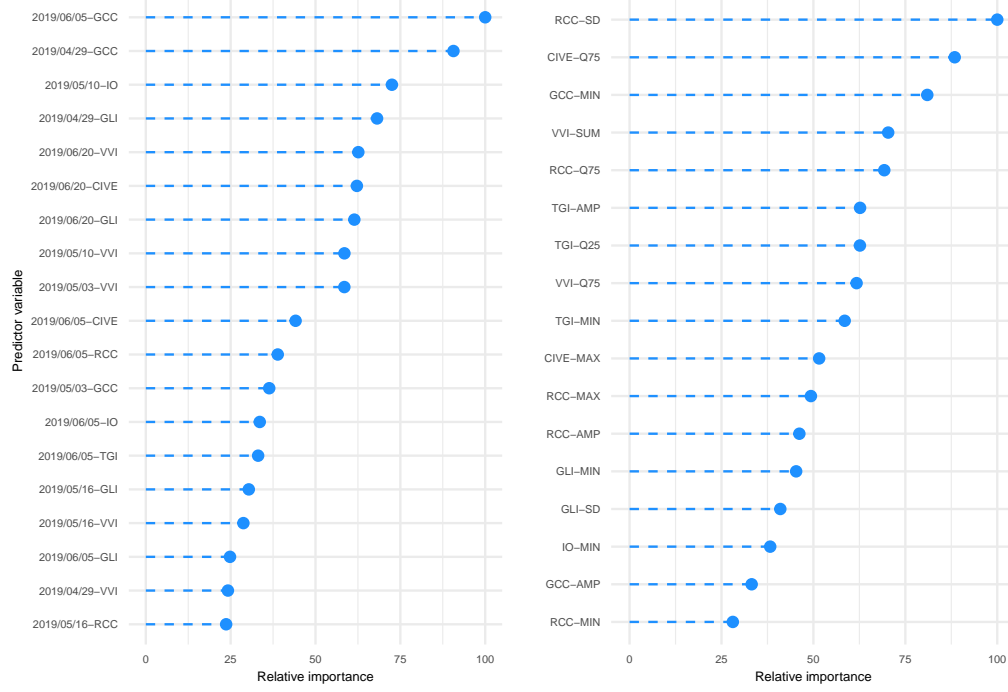


Figure 7: Variable importance for mono-temporal (left) and seasonal (right) predictors averaged across resolutions.

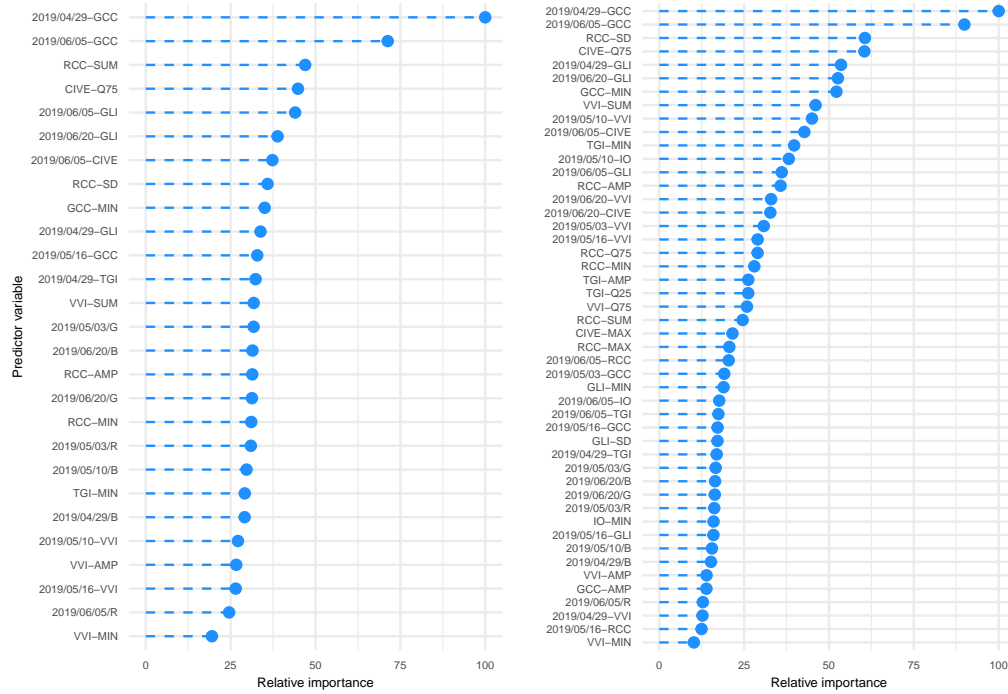


Figure 8: Variable importance for mono-temporal and seasonal predictors averaged across resolutions (left) and averaged variable importance across all model types and resolutions (right).

4 Discussion & Conclusion

By combining mono-temporal and seasonal parameters we were able to achieve an OA of 64.8% at a spatial resolution of 25 cm. It seems that the spatial aggregation of RGB information into coarser resolutions can help to correctly identify tree species. On a pseudo-object based level, without incorporating a true crown delineation, we achieved a maximum OA of 97.1 %. On a pixel basis, we achieve slightly lower OA compared to other studies, conducting similar research in distinct forest environments of the world (Fricker et al., 2019; Natesan et al., 2019; Onishi and Ise, 2018; Sothe et al., 2019).

Onishi and Ise (2018) achieved an OA of 83.1 % by incorporating a tree crown segmentation and training the GoogLeNet neural-network with six different tree species in a forest stand in the warm and humid climate close to Kyoto, Japan. Sothe et al. (2019) achieved a maximum OA of 72.4 % when next to predictor variables of the visible and near infrared spectrum other variables from a photogrammetric point cloud and the canopy height model were included in a support-vector-machine. They differentiated between 12 tree species in a subtropical forest in Southern Brazil. Fricker et al. (2019) used a convolutional-neural-network in a mixed-conifer forest in Northern America and report an F-Score of 64 % for RGB predictors only to differentiate 10 tree species. Natesan et al. (2019) trained a residual network on RGB based predictors to classify between pine trees and non-pine trees in a tree crown segmented image and achieved an OA of 80 %.

When comparing our results to other studies, we have to note that our study area is of less complexity, than for example tropical or sub-tropical forests. We only have two different species in our area and the training data set is slightly unbalanced towards the class of *fagus sylvatica*. This can contribute to an over-classification of this class, leading the trained model to more frequently assign the *fagus sylvatica* class to pixels, and by chance increasing the OA. Next to applying several iterations of cross-validations to account for this error, a more balanced training set could prove useful to achieve more stable results. Concerning the results of the pseudo-object based classification, it is indicated by this study that object-based approaches can significantly increase the OA. As reported by other studies, with the use of neural-networks and a thorough tree crown delineation, very high accuracies can be achieved only based on RGB data even in more complex forest environments (Fricker et al., 2019; Natesan et al., 2019).

Additionally, sources of error in the imagery can have a significant influence on the outcome of a classification process. The images used in this study are prone to a number of sources of errors. Firstly, we observed inconsistencies in the process of georeferencing the images which led to rather large image distortions (Fig. 2). In dense canopy structures, such as our study area, the generation of tie points to correctly match objects from different images, is a function of flight path and height as well as the chosen sensor and can lead to very high margins of error in the localization of pixels (Fraser and Congalton, 2018). Another related issue are the differences in illumination and viewing geometry between several overflights, which seriously limit the comparability of images from different days or even different paths (Fraser and Congalton, 2018; Fricker et al., 2019; Sonnentag et al., 2012). Also, the frequency of overflights is quite high for April and May, however, it is reduced between Mid-May to the end of June, leading to a lower sampling frequency well within the vegetation period. These errors are amplified in the current study by our negligent approach to the localization of individual trees within and across the image time series (Fig. 1). The chosen approach was intended to focus solely on the analysis of the influence of spatial resolution and mono-temporal vs. multi-temporal predictors. However, this makes our results less comparable to other studies and, in fact, useful for practitioners of forestry environmental protection. Without a clear approach to delineate tree crowns and track their development through a time-series of images, the results presented here remain of academic interest only.

The results of the influences of different resolutions and the incorporation of mono- and seasonal-predictors, still have the potential to highlight valid insights. Models trained with both mono-temporal and seasonal indices performed best overall closely followed by models trained with mono-temporal indices. Thus leading us to the conclusion, that mono-temporal predictors are more important than seasonal predictors but a combination of both positively increase the model performance. A reason for the rather poor performance of the seasonal parameters might be the temporal resolution of available UAV overpasses. It is possible that with low-frequency observation flights, the important development processes of vegetation growth and plant senescence might not be captured. Concerning the influence of the spatial resolution, there is an indication that averaging high resolution pixels towards larger spatial units can improve the classification. The results,

however, remain inconclusive when the pixel-based approach is compared to the object-based, since in the latter we observe a decrease in OA above a certain threshold in resolution.

It is thus highly recommended to further analyse the impact of object-based classification strategies on the achievable accuracy. The potential benefit of using low-cost UAVs and sensors for tree species classification is evident, but there remain open question towards which is the most sensible approach to bring this data to efficient uses. To achieve this, a robust scheme of crown delineation seems to be of high importance in order to get a less erroneous training data set. Under these conditions, we suspect the gap between the accuracies of pixel-based and object-based classification methods to be smaller, however, the dynamic of the classification accuracy across changing spatial resolutions seems to be worth to be further investigated.

References

Agisoft, 2019. Agisoft Metashape User Manual 139.

Berra, E.F., Gaulton, R., Barr, S., 2019. Assessing spring phenology of a temperate woodland: A multiscale comparison of ground, unmanned aerial vehicle and Landsat satellite observations. *Remote Sensing of Environment* 223, 229–242. <https://doi.org/10.1016/j.rse.2019.01.010>

Berra, E.F., Gaulton, R., Barr, S., 2016. Use of a digital camera onboard a UAV to monitor spring phenology at individual tree level, in: 2016 Ieee International Geoscience and Remote Sensing Symposium (Igarss). pp. 3496–3499. <https://doi.org/10.1109/IGARSS.2016.7729904>

Breiman, L., 2001. Random forests. *Machine learning* 45, 5–32. <https://doi.org/10.1023/A:1010933404324>

Brieger, F., Herzsuh, U., Pestryakova, L.A., Bookhagen, B., Zakharov, E.S., Kruse, S., 2019. Advances in the derivation of Northeast Siberian forest metrics using high-resolution UAV-based photogrammetric point clouds. *Remote Sensing* 11, 1447. <https://doi.org/10.3390/rs11121447>

Brockerhoff, E.G., Barbaro, L., Castagnyrol, B., Forrester, D.I., Gardiner, B., González-Olabarria, J.R., Lyver, P.O., Meurisse, N., Oxbrough, A., Taki, H., Thompson, I.D., Plas, F. van der, Jactel, H., 2017. Forest biodiversity, ecosystem functioning and the provision of ecosystem services. *Biodiversity and Conservation* 26, 3005–3035. <https://doi.org/10.1007/s10531-017-1453-2>

Broge, N.H., Leblanc, E., 2001. Comparing prediction power and stability of broadband and hyperspectral vegetation indices for estimation of green leaf area index and canopy chlorophyll density. *Remote Sensing of Environment* 76, 156–172. [https://doi.org/10.1016/S0034-4257\(00\)00197-8](https://doi.org/10.1016/S0034-4257(00)00197-8)

Dostálová, A., Wagner, W., Milenković, M., Hollaus, M., 2018. Annual seasonality in Sentinel-1 signal for forest mapping and forest type classification. *International Journal of Remote Sensing* 39, 7738–7760. <https://doi.org/10.1080/01431161.2018.1479788>

Elatawneh, A., Rappl, A., Rehush, N., Schneider, T., Knoke, T., 2013. Forest tree species communities identification using multi phenological stages RapidEye data : case study in the forest of Freising. 5. RESA Workshop 4/2013 1–10.

Food and Agriculture Organsiation of the United Nations, 2015. Global Forest Resources Assessment 2015. <https://doi.org/10.1002/2014GB005021>

Fraser, B.T., Congalton, R.G., 2018. Issues in Unmanned Aerial Systems (UAS) data collection of complex forest environments. *Remote Sensing* 10. <https://doi.org/10.3390/rs10060908>

Fricker, G.A., Ventura, J.D., Wolf, J.A., North, M.P., Davis, F.W., Franklin, J., 2019. A Convolutional Neural Network Classifier Identifies Tree Species in Mixed-Conifer Forest from Hyperspectral Imagery. *Remote Sensing* 11, 2326. <https://doi.org/10.3390/rs11192326>

Frison, P.L., Fruneau, B., Kmiha, S., Soudani, K., Dufrêne, E., Le Toan, T., Koleček, T., Villard, L., Mougin, E., Rudant, J.P., 2018. Potential of Sentinel-1 data for monitoring temperate mixed forest phenology. <https://doi.org/10.3390/rs10122049>

- Gobron, N., Pinty, B., Verstraete, M.M., Widlowski, J.L., 2000. Advanced vegetation indices optimized for up-coming sensors: design, performance, and applications. *IEEE Transactions on Geoscience and Remote Sensing* 38, 2489–2505. <https://doi.org/10.1109/36.885197>
- Grabska, E., Hostert, P., Pflugmacher, D., Ostapowicz, K., 2019. Forest stand species mapping using the sentinel-2 time series. *Remote Sensing* 11, 1–24. <https://doi.org/10.3390/rs11011197>
- Hunt, E.R., Doraiswamy, P.C., McMurtrey, J.E., Daughtry, C.S., Perry, E.M., Akhmedov, B., 2012. A visible band index for remote sensing leaf chlorophyll content at the Canopy scale. *International Journal of Applied Earth Observation and Geoinformation* 21, 103–112. <https://doi.org/10.1016/j.jag.2012.07.020>
- Klosterman, S., Richardson, A.D., 2017. Observing spring and fall phenology in a deciduous forest with aerial drone imagery. *Sensors (Switzerland)* 17. <https://doi.org/10.3390/s17122852>
- Krause, S., Sanders, T.G., Mund, J.P., Greve, K., 2019. UAV-based photogrammetric tree height measurement for intensive forest monitoring. *Remote Sensing* 11, 758. <https://doi.org/10.3390/rs11070758>
- Kuhn, M., 2019. Caret: Classification and regression training, <https://CRAN.R-project.org/package=caret>.
- Laboratory, P.H., 2015. Visible Vegetation Index (VVI).
- Marques, P., Pádua, L., Adão, T., Hruška, J., Peres, E., Sousa, A., Sousa, J.J., 2019. UAV-based automatic detection and monitoring of chestnut trees. *Remote Sensing* 11, 855. <https://doi.org/10.3390/RS11070855>
- Mayer, C., Kersten, T.P., 2018. A Comprehensive Workflow to Process UAV Images for the Efficient Production of Accurate Geo-information A Comprehensive Workflow to Process UAV Images for the Efficient Production of Accurate Geo-information.
- Meyer, H., 2018. CAST: 'Caret' applications for spatial-temporal models, <https://CRAN.R-project.org/package=CAST>.
- Mngadi, M., Odindi, J., Peerbhay, K., Mutanga, O., 2019. Examining the effectiveness of Sentinel-1 and 2 imagery for commercial forest species mapping. *Geocarto International* 0, 1–12. <https://doi.org/10.1080/10106049.2019.1585483>
- Natesan, S., Armenakis, C., Vepakomma, U., 2019. Resnet-based tree species classification using uav images. *International Archives of the Photogrammetry, Remote Sensing and Spatial Information Sciences - ISPRS Archives* 42, 475–481. <https://doi.org/10.5194/isprs-archives-XLII-2-W13-475-2019>
- Nevalainen, O., Honkavaara, E., Tuominen, S., Viljanen, N., Hakala, T., Yu, X., Hyyppä, J., Saari, H., Pölönen, I., Imai, N.N., Tommaselli, A.M., 2017. Individual tree detection and classification with UAV-Based photogrammetric point clouds and hyperspectral imaging. *Remote Sensing* 9. <https://doi.org/10.3390/rs9030185>
- Niculescu, S., Talab Ou Ali, H., Billey, A., 2018. Random forest classification using Sentinel-1 and Sentinel-2 series for vegetation monitoring in the Pays de Brest (France), in: p. 6. <https://doi.org/10.1117/12.2325546>
- Onishi, M., Ise, T., 2018. Automatic classification of trees using a UAV onboard camera and deep learning.
- Persson, M., Lindberg, E., Reese, H., 2018. Tree species classification with multi-temporal Sentinel-2 data. *Remote Sensing* 10, 1–17. <https://doi.org/10.3390/rs10111794>
- Richardson, A.D., Braswell, B.H., Hollinger, D.Y., Jenkins, J.P., Ollinger, S.V., 2009. Near-surface remote sensing of spatial and temporal variation in canopy phenology. *Ecological Applications* 19, 1417–1428. <https://doi.org/10.1890/08-2022.1>
- Rowan, L.C., Mars, J.C., 2003. Lithologic mapping in the Mountain Pass, California area using Advanced Spaceborne Thermal Emission and Reflection Radiometer (ASTER) data. *Remote Sensing of Environment* 84, 350–366. [https://doi.org/10.1016/S0034-4257\(02\)00127-X](https://doi.org/10.1016/S0034-4257(02)00127-X)
- Sonnentag, O., Hufkens, K., Teshera-Sterne, C., Young, A.M., Friedl, M., Braswell, B.H., Milliman, T., O'Keefe, J., Richardson, A.D., 2012. Digital repeat photography for phenological research in forest ecosystems. *Agricultural and Forest Meteorology* 152, 159–177. <https://doi.org/10.1016/j.agrformet.2011.09.009>

- Sothe, C., Dalponte, M., Almeida, C.M. de, Schimalski, M.B., Lima, C.L., Liesenberg, V., Miyoshi, G.T., Tommaselli, A.M.G., 2019. Tree species classification in a highly diverse subtropical forest integrating UAV-based photogrammetric point cloud and hyperspectral data. *Remote Sensing* 11, 1338. <https://doi.org/10.3390/rs11111338>
- Ulsig, L., Nichol, C.J., Huemmrich, K.F., Landis, D.R., Middleton, E.M., Lyapustin, A.I., Mammarella, I., Levula, J., Porcar-Castell, A., 2017. Detecting inter-annual variations in the phenology of evergreen conifers using long-term MODIS vegetation index time series. *Remote Sensing* 9. <https://doi.org/10.3390/rs9010049>
- Wan, L., Li, Y., Cen, H., Zhu, J., Yin, W., Wu, W., Zhu, H., Sun, D., Zhou, W., He, Y., 2018. Combining UAV-based vegetation indices and image classification to estimate flower number in oilseed rape. *Remote Sensing* 10. <https://doi.org/10.3390/rs10091484>
- Yan, W., Guan, H., Cao, L., Yu, Y., Gao, S., Lu, J.Y., 2018. An automated hierarchical approach for three-dimensional segmentation of single trees using UAV LiDAR data. *Remote Sensing* 10, 1999. <https://doi.org/10.3390/rs10121999>
- Yao, H., Qin, R., Chen, X., 2019. Unmanned aerial vehicle for remote sensing applications - A review. <https://doi.org/10.3390/rs11121443>
- Zhang, X., Friedl, M.A., Schaaf, C.B., Strahler, A.H., Hodges, J.C., Gao, F., Reed, B.C., Huete, A., 2003. Monitoring vegetation phenology using MODIS. *Remote Sensing of Environment* 84, 471–475. [https://doi.org/10.1016/S0034-4257\(02\)00135-9](https://doi.org/10.1016/S0034-4257(02)00135-9)